Upper mantle viscosity underneath northern Marguerite Bay, Antarctic Peninsula constrained by bedrock uplift and ice mass variability

Samrat, Nahidul Hoque; King, Matt A.; Watson, Christopher; Hay, Andrea; Barletta, Valentina; Bordoni, Andrea

Published in:
Geophysical Research Letters

Link to article, DOI:
10.1029/2021GL097065

Publication date:
2021

Document Version
Publisher's PDF, also known as Version of record

AGU ADVANCING EARTH AND SPACE SCIENCE

Geophysical Research Letters®

RESEARCH LETTER
10.1029/2021GL097065

Upper Mantle Viscosity Underneath Northern Marguerite Bay, Antarctic Peninsula Constrained by Bedrock Uplift and Ice Mass Variability

Nahidul Hoque Samrat[1,2], Matt A. King[1], Christopher Watson[1], Andrea Hay[1], Valentina R. Barletta[3], and Andrea Bordoni[4]

[1]School of Geography, Planning, and Spatial Sciences, University of Tasmania, Hobart, TAS, Australia, [2]School of Health, Medical and Applied Sciences, Central Queensland University, Bundaberg, QLD, Australia, [3]DTU Space, Technical University of Denmark, Kongens Lyngby, Denmark, [4]DTU Compute, Technical University of Denmark, Kongens Lyngby, Denmark

Abstract We constrain viscoelastic Earth rheology and recent ice-mass change in the northern Marguerite Bay region of the Antarctic Peninsula. Global Positioning System (GPS) time series from Rothera and San Martin stations show bedrock uplift range of ~−0.8–1.8 mm/year over 1999–2005 and 2016–2020 but ~3.5–6.0 mm/year over ~2005–2016. Digital elevation models reveal substantial surface lowering, but at a lower rate since ~2009. Using these data, we show that an elastic-only model cannot explain the non-linear uplift of the GPS sites but that a layered viscoelastic model can. We show close agreement between GPS uplift changes and viscoelastic models with effective elastic lithosphere thickness and upper-mantle viscosity ~10–95 km and ~$0.1–9 \times 10^{18}$ Pa s, respectively. Our viscosity estimate is consistent with a north-south gradient in viscosity suggested by previous studies focused on specific regions within the Antarctic Peninsula and adds further evidence of the low viscosity upper mantle in the northern Antarctic Peninsula.

Plain Language Summary Over the last few decades, the glaciers of the Antarctic Peninsula have thinned tens to hundreds of meters. This unloading of the solid Earth has produced a viscoelastic response of the solid Earth. By observing this response and comparing it to viscoelastic models combined with ice unloading models, we may infer the viscoelastic properties of the Earth in this region. In this study, we estimate ice mass changes over 15 years using satellite images. Then we analyze estimates of solid Earth displacement from continuous Global Positioning System (GPS) stations attached to bedrock. When compared to the predictions of deformation from viscoelastic models with different Earth properties and ice mass change rates, we find the rate of glacier thinning must have slowed since around 2009–2010 and suggests a thin elastic lithosphere with a lower-viscosity upper mantle underneath this region.

Key Points:

- GPS-measured time-varying uplift rates ranging between ~1.6 ± 0.8 and ~6.0 ± 0.6 mm/year over 1999.1–2016.0 in Northern Marguerite Bay
- Glaciers in the region generally show a reduced rate of surface lowering since ~2009
- Comparing GPS and modeled viscoelastic deformation suggests a lower-viscosity upper mantle for this region with possible thin lithosphere

Supporting Information:

Supporting Information may be found in the online version of this article.

Correspondence to:

N. H. Samrat,
nahidul.samrat@utas.edu.au

Citation:

Samrat, N. H., King, M. A., Watson, C., Hay, A., Barletta, V. R., & Bordoni, A. (2021). Upper mantle viscosity underneath northern Marguerite Bay, Antarctic Peninsula constrained by bedrock uplift and ice mass variability. *Geophysical Research Letters*, *48*, e2021GL097065. https://doi.org/10.1029/2021GL097065

Received 15 NOV 2021
Accepted 17 NOV 2021

Author Contributions:

Conceptualization: Nahidul Hoque Samrat, Matt A. King, Christopher Watson
Formal analysis: Nahidul Hoque Samrat, Andrea Hay
Investigation: Nahidul Hoque Samrat, Matt A. King, Andrea Hay
Methodology: Nahidul Hoque Samrat, Matt A. King
Resources: Nahidul Hoque Samrat, Valentina R. Barletta, Andrea Bordoni
Software: Valentina R. Barletta, Andrea Bordoni
Supervision: Matt A. King, Christopher Watson
Validation: Nahidul Hoque Samrat
Visualization: Nahidul Hoque Samrat
Writing – original draft: Nahidul Hoque Samrat

1. Introduction

The Antarctic Peninsula (AP) experienced rapid regional warming over the last half of the 20th Century. This warming is expressed in both the atmosphere and ocean temperature records and model reanalyses since ~1950 (Cook et al., 2016; Turner et al., 2005, 2016). This has led to the substantial retreat and collapse of multiple major ice shelves in the western and eastern sides of the Peninsula (Fox & Vaughan, 2005; Rack & Rott, 2004; Rott et al., 1996; Scambos et al., 2004). The outlet glaciers have exhibited rapid acceleration and dynamic thinning in response to the disintegration of ice shelves. This ice unloading has resulted in a rapid viscoelastic solid Earth response, captured by Global Positioning System (GPS) stations fixed to bedrock in the northern Antarctic Peninsula (Nield et al., 2014; Samrat et al., 2020) while in the southern Antarctic Peninsula, the bedrock deformation seems to reflect ice loading changes over longer timescales (Wolstencroft et al., 2015; Zhao et al., 2017). Combined with viscoelastic models, these studies have together suggested that the region is underlain by the upper mantle with low viscosity ($0.1–3 \times 10^{18}$ Pa s) in the north but increasing to more conventional values ($>2 \times 10^{19}$ Pa s) in the southern Peninsula. These provide constraints on models of glacial isostatic adjustment (GIA); accurate models of GIA are essential to accurately understanding the ice sheet contribution to sea-level change from space-gravimetry data (King et al., 2012).

Here, we examine a previously unstudied region of the Antarctic Peninsula, approximately midway between the northern and southern regions previously studied in northern Marguerite Bay (NMB). The glaciers in this

Writing – review & editing: Nahidul Hoque Samrat, Matt A. King, Christopher Watson, Andrea Hay, Valentina R. Barletta, Andrea Bordoni

region have undergone general retreat and modest levels of lowering over the second half of the 20th Century (Cook, 2014; Kunz et al., 2012; Pritchard & Vaughan, 2007). Continuous GPS deployments in this region now span 20 years. One of these, located at Rothera Station (ROTH; Figure 1), was studied by Thomas et al. (2011), who found a rate of uplift of ∼1.7 and 6.5 mm/year in 2000 and 2006, respectively, but was unable to explain this rate with an elastic only model forced with a low-resolution ice model. A rate of uplift of ∼6.5 mm/year is much larger than any current model of millennial-scale GIA (Martín-Español et al., 2016), so this uplift rate remains unexplained. Another three GPS sites, SMRT, SMR5, and BSA1, were deployed in 1999, 2009, and 2012 respectively, about 60–70 km south-east of ROTH at Horseshoe Island (BSA1) and Millerand Island (SMRT, SMR5), as shown in Figure 1. We study the time series of these four sites in the context of regional ice loading changes and consequent solid Earth deformation.

This paper describes the estimation of ice surface elevation change around the NMB region using new digital elevation models covering ∼2001 to 2017 in the region shown in Figure 1. We then use the derived ice loading data to predict the solid Earth response using a suite of viscoelastic models and compare them with GPS observations. The comparison with GPS enables us to place constraints on the solid Earth rheology in this region and compare it to the adjoining regions to the north and south.

2. Data and Methods

2.1. Ice Surface Elevation Change

Recent decadal-scale ice elevation changes have been studied in detail in some of the areas in AP (e.g., northern AP adjacent to the former Larsen B Ice Shelf and the southern part of Marguerite Bay adjacent to the Fleming Glacier), but the NMB area is yet to be considered. The glaciers within the area of NMB are less than 20 km in length, and there are two small ice shelves in this area: Muller and Jones ice shelves. The Muller Ice Shelf is the northern-most ice shelf located at the embayment of Lallemand Fjord on the west side of the AP. It is a small ice shelf with an area of ∼80 km^2. This ice shelf is mainly fed by the Antevs and Bruckner glaciers (Domack et al., 1995), and its front has been in retreat since ∼1947, with the notable exception of two advances in 1956 and 1986 (Cook & Vaughan, 2010). Cook (2014) showed that the ice shelf lost almost 49% of its area over 1950–2008 due to regional climate change. The Jones Ice Shelf was located ∼25 km south of Muller Ice Shelf. This ice shelf began to retreat in the early 1970 and completely disappeared in early 2003. The effect on glacier dynamics is not yet observed around this area. This area is also subject to strong surface mass-balance fluctuations.

To develop a time series of glacier Digital Elevation Models (DEMs), we used Advanced Spaceborne Thermal Emission and Reflection Radiometer (ASTER) data for 2002–2017. We downloaded ASTER Level 1A (L1A) 30 m resolution data through the NASA Earthdata portal in GeoTIFF format. Based on image coverage of our study area, we divided our area into eastern and western sectors. A detailed description of our approach to producing ice mass changes using ASTER data is found in Text S1 in Supporting Information S1.

2.2. GPS

We considered GPS data from sites with near-continuous records in the region, namely Rothera and San Martin which commenced measurements in the late 1990s, and the Horseshoe Harbour site deployed in 2012 (Figure 1). The GPS records considered span 1999.1–2020.0 (ROTB/ROTH), 2012.1–2020.0 (BSA1), 1999.3–2009.2 (SMRT/SMR5) and 2009.2–2020.0 (SMR5). Further information on GPS data processing is found in Text S2 in Supporting Information S1.

There are two separate GPS records (ROTH, ROTB) at Rothera station, which we merge to produce the record we refer to as ROTH for convenience hereafter. ROTB covers the period from ∼1999.1 until 2011.16, while ROTH has operated since ∼2010.10. We estimated and removed the offset between the two series using the final 20 days of overlapping data. The two records at San Martin (SMRT and SMR5) do not have substantial overlapping data, and we therefore treat them as distinct records.

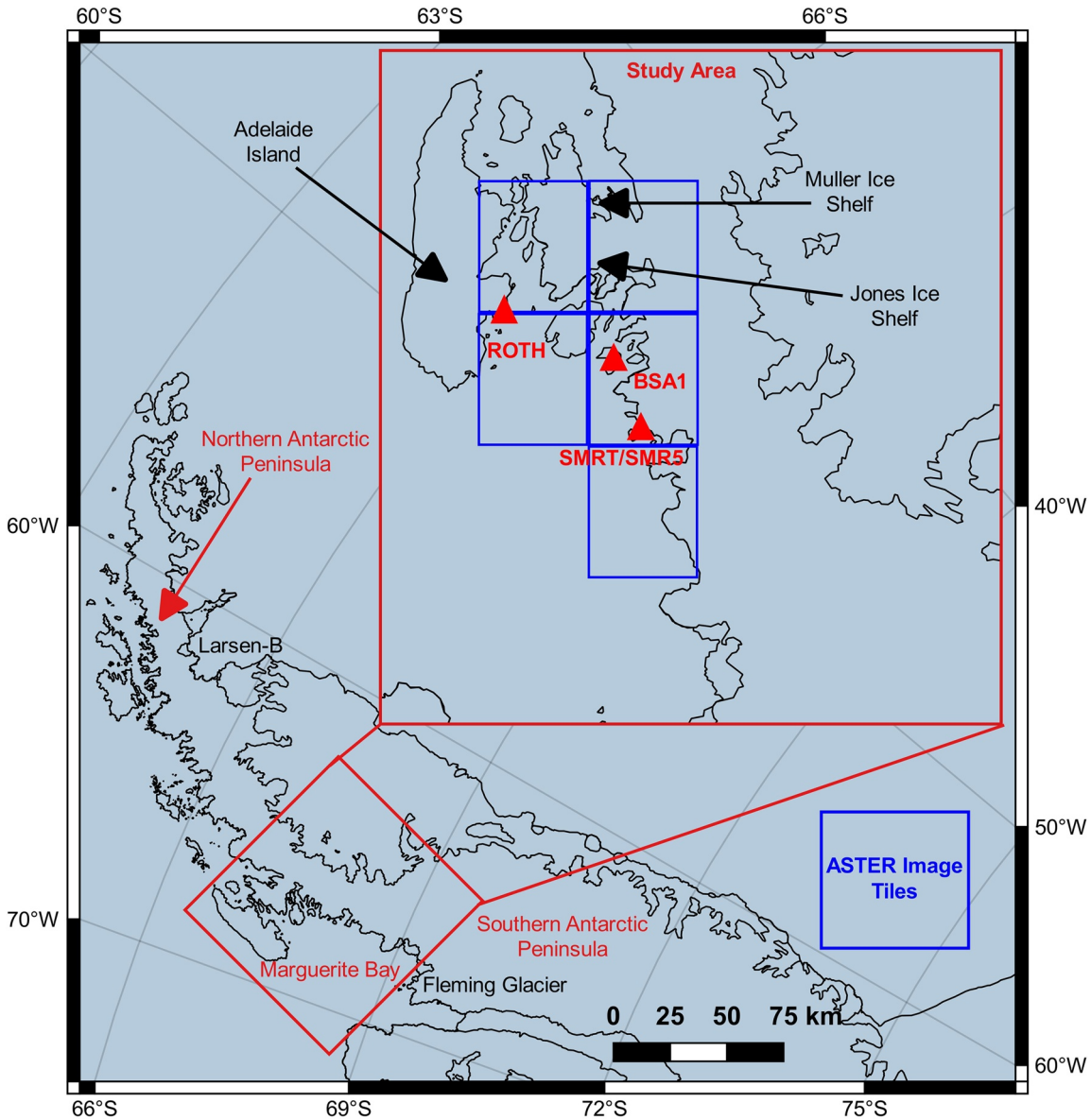

Figure 1. Location map of our study area with Global Positioning System site locations at Rothera station (ROTH), Horseshoe Island (BSA1), and San Martin station (SMRT and SMR5 marked). The Mosaic of Antarctica (MOA) data set was used to define the grounding line (Haran et al., 2014).

2.3. Viscoelastic Solid Earth Modeling

We follow the same methodology as Nield et al. (2014) and Samrat et al. (2020) to model the solid Earth response to changes in surface loading. In brief, this involved the computation of both elastic and viscous deformations using the elastic and viscous components of the Green Functions computed with VE-CL0V3RS v3.6 (Visco-Elastic Compressible LOVe numbER Solver) successively convoluted with the loading function using VE-HresV2 (Visco-Elastic High-Resolution technique for Earth deformations) software (Barletta et al., 2006, 2018; DTU, 2021). Further information is found in Text S3 in Supporting Information S1.

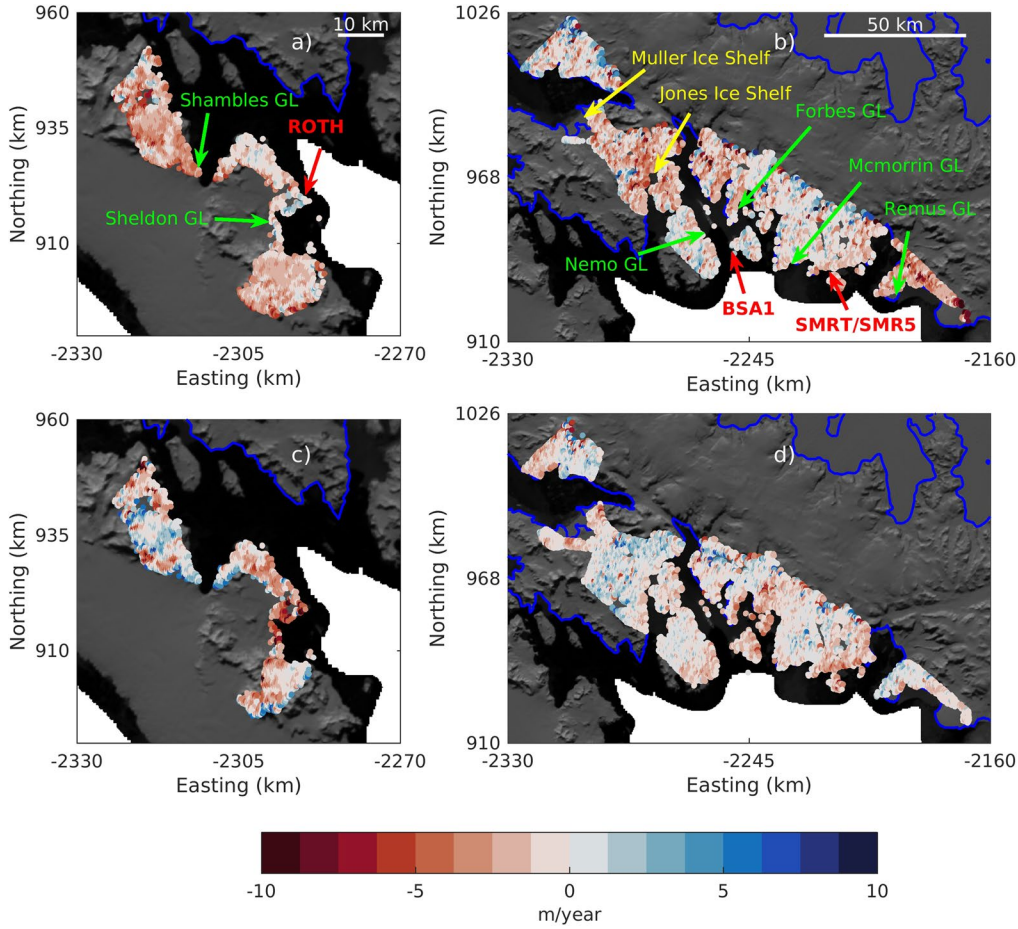

Figure 2. Elevation change rate over, (a) the western part between 2004.0 and 2012.0, (b) the eastern part between 2002.0 and 2009.0, (c) the western part between 2012.0 and 2017.0, and (d) the eastern part between 2009.0 and 2015.0. The blue line shows the grounding line.

3. Results

3.1. Glacier Elevation Changes and Mass Balance

We estimate the elevation change rates for the eastern and western parts of our study area using linear rates of surface elevation change over each period 2002.0–2009.0 and 2009.0–2015.0 for the eastern part, and 2004.0–2012.0 and 2012.0–2017.0 for the western part. The elevation change rate is shown in Figure 2 for the eastern and western parts of the study area.

The eastern part shows an overall volume loss of 7,039 ± 1.3 km^3 (1-sigma uncertainties) during 2002.0–2009.0 and subsequently, 1,371 ± 10 km^3 over the period 2009.0–2015.0. The western part shows a similar pattern, with an overall volume loss of 2,709 ± 3.2 km^3 over 2004.0–2012.0, followed by ~764 ± 1 km^3 over 2012.0–2017.0. These estimations consider only the sampled areas (Figures 2a–2c) and do not include changes in data gaps.

The elevation change in Figure 2b shows a positive surface elevation change rate during 2009.0–2015.0 near the Jones Ice Shelf. Comparing it to Figure 2a suggests that the thinning rate of the glaciers around the broader area slowed down during that period. A similar spatial pattern of mass change was also noticeable in the Muller Ice Shelf area, and it indicates that thinning rates of glaciers around this ice shelf have reduced since ~2009. The area near Shambles (Figures 2a and 2c) and Remus glaciers (Figures 2b and 2d) show an elevation change rate close to zero between 2009–2015 and 2012–2017, respectively, suggesting a reduction in the rate of surface elevation change since the earlier period. The Sheldon, Mcmorrin, Nemo, and Forbes glacier regions (Figure 2) show an almost constant rate of elevation change pattern through 2002.0–2015.0. The most considerable surface elevation

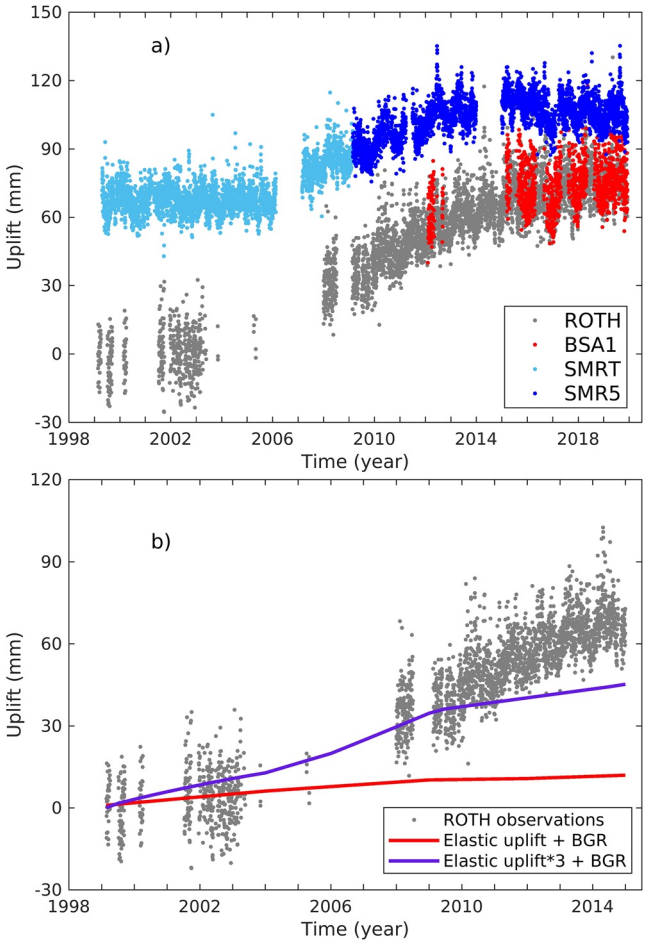

Figure 3. (a) Global Positioning System (GPS) uplift time series for the merged ROTH, BSA1, SMRT and SMR5 sites. Time series are arbitrarily shifted vertically for clarity, and (b) ROTH GPS observations are compared with the uplift time series predicted by the elastic model and BGR applied over the period where the model has ice loading data.

change is near the Remus Glacier region, which we find to have lowered by ~5.8 m/year over 2002.0–2009.0.

The ice mass change estimated from the elevation change data (before gap filling, Text S1 in Supporting Information S1 for detail about our gap-filling approach) over each period is presented in Table S2 in Supporting Information S1. The area-integrated mass unloading is smaller over 2009.0–2015.0 than the earlier 2002.0–2009.0. The negative mass balance indicates that mass loss is ongoing from 2002.0 to 2015.0, although its rate reduces since ~2009.0. Figure S1 in Supporting Information S1 shows surface elevation changes over time at a range points close to the GPS sites.

3.2. GPS Results and Model Fit Analysis

Figure 3a shows the bedrock uplift time series for the ROTH, BSA1, SMRT, and SMR5 sites with arbitrary vertical shifts applied for clarity. The four-time series show non-linear rates of uplift and have similar patterns over their common time periods. The uplift rates and their uncertainties are shown for different time periods in Table S3 in Supporting Information S1.

The uplift of the San Martin site (SMRT/SMR5) is ~−0.9 ± 0.3 mm/year over 1999.3–2005.0 but increases dramatically after ~2005.0 to ~6.0 ± 0.6 mm/year before leveling off after ~2016 to ~0.8 ± 0.9 mm/year. At ROTH, the maximum uplift reaches almost 5.9 ± 0.9 mm/year during 2005.0–2010.0, but this rate slightly reduces to ~4.6 ± 0.6 mm/year during ~2010.0–2016.0 and dramatically reduces to ~1.8 ± 1.3 mm/year during ~2016.0–2020.0. The GPS observations from ROTH and SMRT show the same trend of rates over their common periods ~1999–2009, but SMRT has slightly lower uplift rates than ROTH during their common period. However, the ROTH record is patchy during this period. BSA1 shows a similar pattern to the other sites over ~2012.0–2015.0 with ~4.6 ± 0.6 mm/year (ROTH), ~3.5 ± 0.5 mm/year (SMR5), and ~4.3 ± 0.5 mm/year (BSA1) uplift rates over ~2010.0–2016.0, ~2009.2–2016.0 and ~2012.1–2016.0, respectively. However, the apparent downwards trend after 2015 seems slightly stronger at SMR5 and BSA1 than at ROTH, although the BSA1 record is quite short and hence the rate is relatively uncertain.

Assuming this is due to ice mass loading changes, this result suggests that mass loss in the area has slowed or even switched to mass gain in recent years in a period where we do not have DEMs. Overall, ROTH shows ~4.3 ± 0.2 mm/year uplift over 1999.1–2020.0, BSA1 shows ~2.1 ± 0.4 mm/year over 2012.1–2020.0, SMRT shows ~1.8 ± 0.4 mm/year over 1999.3–2009.2 and SMR5 show ~1.4 ± 0.4 mm/year over 2009.2–2020.0, but the rates are clearly not linear, and therefore not an indication of millennial-scale GIA uplift.

In this study, we considered in our modeling only the very recent ice unloading history estimated using ASTER data since ~2002.0. Our GPS time series might have additional deformation driven by ice unloading history not considered in our ice loading model (e.g., due to LGM deglaciation) and we define this as the background rate (BGR). We estimate this rate for each model following the approach of Zhao et al. (2017). In brief, we estimated the background (pre-1999) vertical velocity by computing the difference between observed and predicted uplift rates at ROTH and SMRT. This background rate is then added to our various predicted uplift rates.

We compare the GPS observation with the prediction from the numerical models up to ~2015.0 to match our input ice loading history. Also, from here, we focus on only the ROTH and SMRT sites because these two sites cover the more extended period of input ice loading history considered in this study.

In Figure 3b we compare our GPS uplift time series to the elastic-only model of deformation for the long-running site ROTH. The changing uplift rates recorded at ROTH cannot be explained by elastic prediction only (red line)

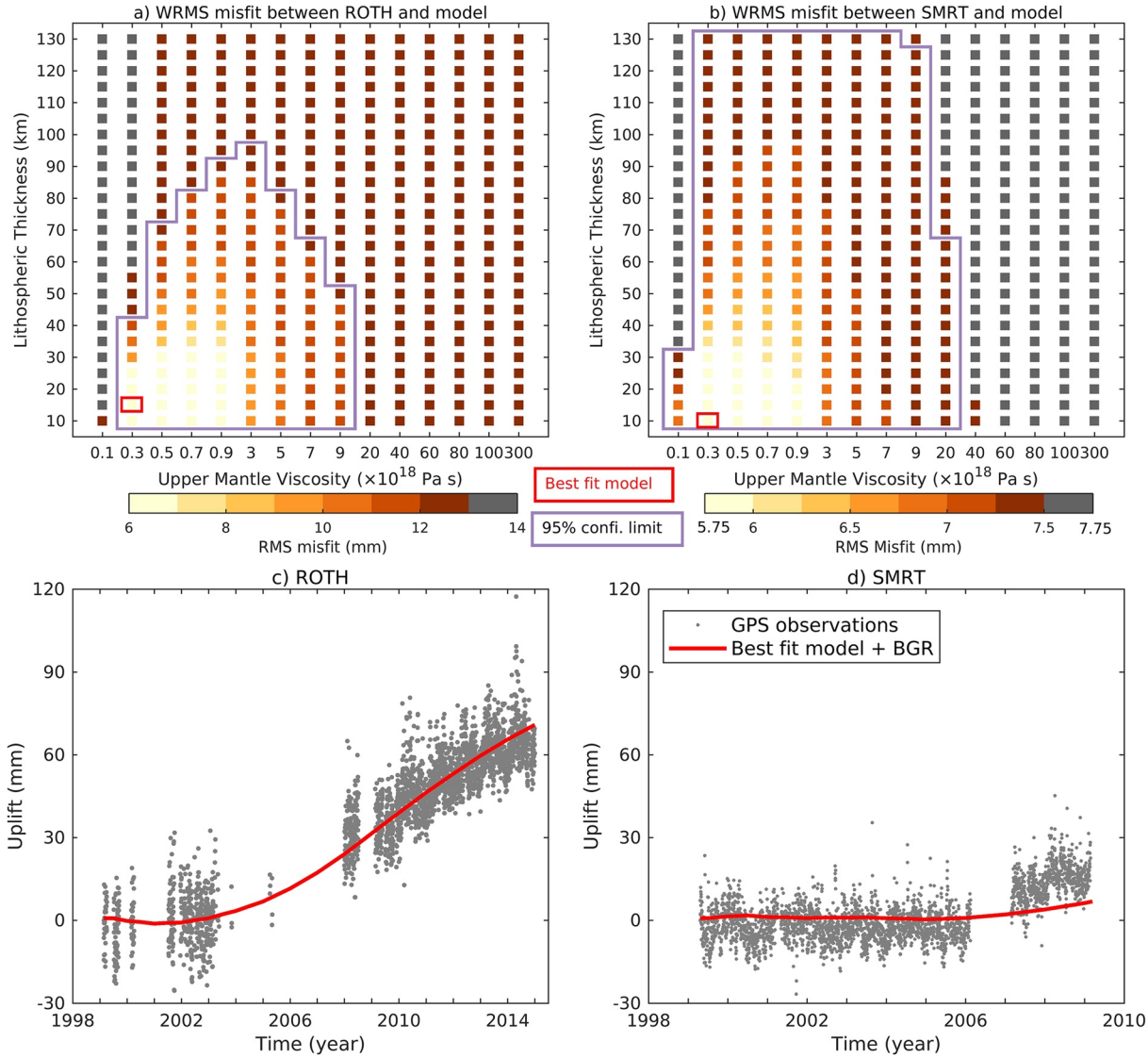

Figure 4. (a) WRMS misfit between ROTH Global Positioning System (GPS) and model-predicted uplift based on fitting to ROTH, (b) WRMS misfit between SMRT GPS and model-predicted uplift based on fitting to SMRT. GPS observations and model predicted uplift time-series for the best fitting viscoelastic Earth model for (c) ROTH and (d) SMRT sites based on the best fitting ROTH model (red square in Figure 4a; LT 15 km and UMV $\sim 3 \times 10^{17}$ Pa s). The model prediction includes the viscoelastic deformation plus the computed BGR for each site.

and this remains true even when the observed mass loss is increased by a factor of more than three (shown by the purple line in Figure 3b). So much missing ice, sustained over the full period is not reasonable, so we reject the possibility of missing ice unloading in our model being the major reason for this. We now explore additional deformation from the viscous model as a means of explaining the remaining GPS uplift.

We compared the ROTH and SMRT uplift time-series with the set of predicted visco-elastic responses computed using 375 viscoelastic numerical Earth models varying lithospheric thickness (LT, by 10–130 km) and Upper Mantle Viscosity (UMV from 0.1 to 300×10^{18} Pa s). We estimated the RMS misfit between the GPS and model (including the BGR) uplift time-series for each station by considering the data uncertainties (that is, the weighted RMS, WRMS, see Text S4 in Supporting Information S1). The WRMS misfit between the GPS observed uplift and modeled predictions is shown in Figures 4a and 4b for ROTH and SMRT sites.

Analysis at the ROTH site shows good agreement with models using upper-mantle viscosities of ~ 0.1–9×10^{18} Pa s and effective thicknesses of the lithosphere within the range of ~10–95 km. The minimum WRMS misfit is found for LT 15 km with UMV of $\sim 3 \times 10^{17}$ Pa s for the ROTH site (Figure 4a). The BGR for the preferred model

is −1.3 mm/year at ROTH. Repeating the analysis for the short SMRT record demonstrates a similar UMV range to the ROTH analysis but shows poor sensitivity to the effective thicknesses of the lithosphere (see Figure 4b). The minimum WRMS misfit for SMRT is found for LT 10 km with UMV of $\sim 3 \times 10^{17}$ Pa s. The BGR for this model is ∼−0.3 mm/year at SMRT. The best fit model from SMRT is almost similar to the best-fit Earth model suggested by the ROTH site. But this site has a short time series which makes the analysis more sensitive to short-term GPS fluctuations. The SMRT site is also closer to the glaciers with changing mass.

The deformation prediction based on the best fitting Earth model constraint from the ROTH analysis (LT = 15 and UMV = 3×10^{17} Pa s) reproduces the uplift quite well for both sites as shown in Figures 4c and 4d (red line), although with an under-prediction at SMRT.

Our study area is small, and all the GPS sites are less than ∼70 km from each other and are each located close to areas of significant mass loss area. Our GPS uplift rates shown in Table S3 in Supporting Information S1 reveal that the GPS observations from ROTH, SMRT/SMR5, and BSA1 show the same trend of rates over their common periods. Given the load change is spatially variable within our study region, this suggests the solid Earth response is not highly short wavelength. To further illustrate this, we recomputed the time series of uplift at ROTH using only the ice load further than ∼15 km radius from ROTH (Figure S2 in Supporting Information S1), indicating that much of the signal at ROTH comes from the wider region.

4. Discussion

Our best-fitting viscoelastic models closely match the GPS-observed bedrock uplift at ROTH and SMRT sites. The analysis shows a preference for a very thin elastic lithosphere could indicate missing ice mass loss, although also note that a wide range of thicknesses is permissible. The confidence intervals are shown in Figures 4a and 4b (purple color) assume that the data are temporally uncorrelated and the model is based on a complete ice loading history. This results in a conservative estimate of the uncertainty bounds, including more Earth models than may closely fit the GPS data (see ROTH observations with the prediction from the models fall within 95% confidence limit in Figure S3 in Supporting Information S1). To investigate this further, we adopt model fit analysis for ROTH observations based on sub-period velocity shown in Table S3 in Supporting Information S1 (∼1999.1–200.5, ∼2005.0–2010.0, and ∼2010.0–2016.0). This analysis rules out a few models from the range estimated considering the whole time series of ROTH (purple line in Figure S4a; Figure S4 in Supporting Information S1), but does not provide a major reduction in the range of plausible Earth models.

To estimate further how ice loading changes in nearby regions could affect deformation in NMB we add the ice loading model of the Larsen-B and Fleming Glacier regions from Samrat et al. (2020) and Zhao et al. (2017) with our loading model (see Text S5 and Figure S5 in Supporting Information S1 for detail about the test).

Studies by Samrat et al. (2020), Zhao et al. (2017), and Wolstencroft et al. (2015) estimated UMVs of $<9 \times 10^{18}$, $>2 \times 10^{19}$, and $1–3 \times 10^{20}$ Pa s, for the northern Antarctic Peninsula, Fleming Glacier area (southern Margeurite Bay), and Palmer Land (further south) respectively. Together, these three studies suggest a north-south gradient of UMV exists in the AP. Our suggested UMV range ($\sim 0.1–20 \times 10^{18}$ Pa s) is consistent with these findings given the study site location (north of Fleming Glacier and south of the northern Antarctic Peninsula).

We also note that our modeling considers a simple linear Maxwell rheology, also because there are insufficient data to test more complex (e.g., transient, power-law) models. In particular, Ivins et al. (2020) have highlighted that rheological models which include transient deformation could be an alternative explanation for the low viscosities suggested by GPS-model comparisons in Antarctica. This remains the subject of important future research.

Our estimates of the background rate of uplift is lower than predicted by millennial-scale GIA models. A higher uplift rate from ∼+1 to +5.5 mm/year is predicted for the study area by the different GIA models (Martín-Español et al., 2016). In contrast, our estimates of pre-1999 uplift rates for best fit models are ∼−1.3 and −0.3 mm/year (our estimation of BGR for all models demonstrate subsidence rates of up to ∼1.8 mm/year for this region, see Figure S6 in Supporting Information S1), given the preference for low mantle viscosity with thin lithosphere in our tests. Therefore, it is likely that uplift rates at these sites are more sensitive to mass changes in the decades (Nield et al., 2012), rather than millennia, before 1999, the signal for which is not included in millennial-scale GIA models and is poorly constrained by observations.

The error analysis for our ice mass balance estimates was limited to investigating the elevation residuals over the stable terrain (see Text S6 and Figure S7 in Supporting Information S1). Our results do not include a full ice elevation change error analysis, and these are not propagated through the viscoelastic model; the limited temporal sampling of the DEMs probably dominates any such error combined with uncertainty in the adopted density used to convert to mass. More regular (e.g., annual) DEMs from higher-resolution sensors and density estimation from a densification model would allow a tighter constraint on the model, and perhaps separation of models with more complex rheological structures. For density, we adopt a density of ice when converting elevation change to mass change; changing to a lower density would require even weaker Earth models to reproduce the observed changes in uplift rates.

5. Conclusions

We studied the ice elevation change in the region around northern Marguerite Bay using six DEMs covering a total of 15 years over the period 2002–2004 to 2015–2017. The data suggest a negative mass balance over 2002–2004 to 2009–2012, followed by a reduction in mass loss since ∼2009.0 and 2012.0 for the eastern and western parts of the study area, respectively.

Bedrock GPS time series in the area show non-linear station motion that increases during 2005–2009/10 compared to 1999–2005, and starts reducing from ∼2016. These changes cannot be reproduced by deformation predicted using an elastic-only model forced by our ice loading data, but can be closely reproduced with a range of viscoelastic models. Therefore, we conclude that the sites respond to viscoelastic deformation due to contemporary ice mass change, with additional deformation due to earlier changes in surface loading.

A comparison of the model predicted uplift with the longer GPS (ROTH) time series suggests an upper mantle viscosity of $\sim 0.1–9 \times 10^{18}$ Pa s with ∼10–95 km range lithospheric thickness. The analysis of SMRT shows broad agreement with the ROTH results, but with reduced sensitivity to the lithospheric thickness and upper mantle viscosity.

An improved ice loading model and more extended GPS time series could help to resolve the solid Earth properties further for the region. Our suggested viscosity range agrees with previous studies, indicating a broad north-south gradient in upper mantle viscosity in the Antarctic Peninsula. The specific solid Earth properties of this region still remain to be defined tightly, but our investigation sets an approximate range for upper-mantle viscosity and lithospheric thickness, which will help to understand more complex features of the solid Earth of this region in the future.

Data Availability Statement

GPS data used in this study were downloaded from public archives at UNAVCO (https://www.unavco.org/data/data.html), International GNSS Service (https://www.igs.org/data-products-overview/#products-related-resources) and PANGEA (Schenke et al., 2012), while SMRT data were provided by Andres Zakrajsek and Hans-Werner Schenke. GPS, surface elevation change, and Viscoelastic models data used in this paper are available at: https://rdp.utas.edu.au/metadata/6c5dd3ac-529a-42cb-94a8-44bc39d47aa0.

Acknowledgments
N. H. S. was a recipient of an Australian Government Research Training Program Scholarship. The authors thank the Jet Propulsion Laboratory, NASA, for openly providing ASTER data; these data are freely available at https://search.earthdata.nasa.gov/. M.A.K. was supported by an Australian Research Council Future Fellowship (project number FT110100207) and the Australian Research Council's Special Research Initiative for Antarctic Gateway Partnership (Project ID SR140300001). VE-CL0V3RS is a self-funded project by V.R.B and A.B. The BSA1 site was deployed by the British Services Antarctic Expedition 2012. We thank British Antarctic Survey for supporting the maintenance of ROTH and BSA1. The authors thank to Editor Dr. Lucy Flesch and two anonymous reviewers for critically reading the manuscript and suggesting substantial improvements.

References

Barletta, V. R., Bevis, M., Smith, B. E., Wilson, T., Brown, A., Bordoni, A., et al. (2018). Observed rapid bedrock uplift in Amundsen Sea Embayment promotes ice-sheet stability. *Science*, *360*, 1335–1339. https://doi.org/10.1126/science.aao1447

Barletta, V. R., Ferrari, C., Diolaiuti, G., Carnielli, T., Sabadini, R., & Smiraglia, C. (2006). Glacier shrinkage and modeled uplift of the Alps. *Geophysical Research Letters*, *33*, L14307. https://doi.org/10.1029/2006gl026490

Cook, A. (2014). *Spatial and temporal changes in marine-terminating glaciers on the Antarctic Peninsula since the 1940s*. Swansea University.

Cook, A., Holland, P., Meredith, M., Murray, T., Luckman, A., & Vaughan, D. (2016). Ocean forcing of glacier retreat in the western Antarctic Peninsula. *Science*, *353*, 283–286. https://doi.org/10.1126/science.aae0017

Cook, A. J., & Vaughan, D. G. (2010). Overview of areal changes of the ice shelves on the Antarctic Peninsula over the past 50 years. *The Cryosphere*, *4*, 77–98. https://doi.org/10.5194/tc-4-77-2010

Domack, E. W., Ishman, S. E., Stein, A. B., Mcclennen, C. E., & Jull, A. T. (1995). Late Holocene advance of the Müller ice shelf, Antarctic Peninsula: Sedimentological, geochemical and palaeontological evidence. *Antarctic Science*, *7*, 159–170. https://doi.org/10.1017/s0954102095000228

DTU. (2021). *DTU computing center resources*. DTU. https://doi.org/10.48714/DTU.HPC.0001

Fox, A. J., & Vaughan, D. G. (2005). The retreat of Jones ice shelf, Antarctic Peninsula. *Journal of Glaciology*, *51*, 555–560. https://doi.org/10.3189/172756505781829043

Haran, T., Bohlander, J., Scambos, T., Painter, T., & Fahnestock, M. (2014). *MODIS mosaic of Antarctica 2008–2009 (MOA2009) image map*. [Coastlines, Grounding Lines, and Islands]. https://doi.org/10.7265/N5KP8037

Ivins, E. R., Caron, L., Adhikari, S., Larour, E., & Scheinert, M. (2020). A linear viscoelasticity for decadal to centennial time scale mantle deformation. *Reports on Progress in Physics*, *83*(10), 106801. https://doi.org/10.1088/1361-6633/aba346

King, M. A., Bingham, R. J., Moore, P., Whitehouse, P. L., Bentley, M. J., & Milne, G. A. (2012). Lower satellite-gravimetry estimates of Antarctic sea-level contribution. *Nature*, *491*, 586. https://doi.org/10.1038/nature11621

Kunz, M., King, M. A., Mills, J. P., Miller, P. E., Fox, A. J., Vaughan, D. G., & Marsh, S. H. (2012). Multi-decadal glacier surface lowering in the Antarctic Peninsula. *Geophysical Research Letters*, *39*, L19502. https://doi.org/10.1029/2012gl052823

Martín-Español, A., King, M. A., Zammit-Mangion, A., Andrews, S. B., Moore, P., & Bamber, J. L. (2016). An assessment of forward and inverse GIA solutions for Antarctica. *Journal of Geophysical Research: Solid Earth*, *121*, 6947–6965. https://doi.org/10.1002/2016JB013154

Nield, G. A., Barletta, V. R., Bordoni, A., King, M. A., Whitehouse, P. L., Clarke, P. J., et al. (2014). Rapid bedrock uplift in the Antarctic Peninsula explained by viscoelastic response to recent ice unloading. *Earth and Planetary Science Letters*, *397*, 32–41. https://doi.org/10.1016/j.epsl.2014.04.019

Nield, G. A., Whitehouse, P. L., King, M. A., Clarke, P. J., & Bentley, M. J. (2012). Increased ice loading in the Antarctic Peninsula since the 1850s and its effect on glacial isostatic adjustment. *Geophysical Research Letters*, *39*, L17504. https://doi.org/10.1029/2012gl052559

Pritchard, H. D., & Vaughan, D. G. (2007). Widespread acceleration of tidewater glaciers on the Antarctic Peninsula. *Journal of Geophysical Research*, *112*(F3), F03S29. https://doi.org/10.1029/2006jf000597

Rack, W., & Rott, H. (2004). Pattern of retreat and disintegration of the Larsen B ice shelf, Antarctic Peninsula. *Annals of Glaciology*, *39*, 505–510. https://doi.org/10.3189/172756404781814005

Rott, H., Skvarca, P., & Nagler, T. (1996). Rapid collapse of northern Larsen ice shelf, Antarctica. *Science*, *271*, 788–792. https://doi.org/10.1126/science.271.5250.788

Samrat, N. H., King, M. A., Watson, C., Hooper, A., Chen, X., Barletta, V. R., & Bordoni, A. (2020). Reduced ice mass loss and three-dimensional viscoelastic deformation in northern Antarctic Peninsula inferred from GPS. *Geophysical Journal International*, *222*(2), 1013–1022. https://doi.org/10.1093/gji/ggaa229

Scambos, T. A., Bohlander, J., Shuman, C. U., & Skvarca, P. (2004). Glacier acceleration and thinning after ice shelf collapse in the Larsen B embayment, Antarctica. *Geophysical Research Letters*, *31*, L18402. https://doi.org/10.1029/2004gl020670

Schenke, H. W., Zakrajsek, A. F., Vey, S., & Krocker, R. (2012). *Position measurements at GPS station SMR5*. Alfred Wegener Institute, Helmholtz Centre for Polar and Marine Research. https://doi.org/10.1594/PANGAEA.770301

Thomas, I. D., King, M. A., Bentley, M. J., Whitehouse, P. L., Penna, N. T., Williams, S. D., et al. (2011). Widespread low rates of Antarctic glacial isostatic adjustment revealed by Gps observations. *Geophysical Research Letters*, *38*, L22302. https://doi.org/10.1029/2011gl049277

Turner, J., Colwell, S. R., Marshall, G. J., Lachlan-Cope, T. A., Carleton, A. M., Jones, P. D., et al. (2005). Antarctic climate change during the last 50 years. *International Journal of Climatology*, *25*, 279–294. https://doi.org/10.1002/joc.1130

Turner, J., Lu, H., White, I., King, J. C., Phillips, T., Hosking, J. S., et al. (2016). Absence of 21st century warming on Antarctic Peninsula consistent with natural variability. *Nature*, *535*, 411. https://doi.org/10.1038/nature18645

Wolstencroft, M., King, M. A., Whitehouse, P. L., Bentley, M. J., Nield, G. A., King, E. C., et al. (2015). Uplift rates from a new high-density Gps network in Palmer Land indicate significant late Holocene ice loss in the southwestern Weddell Sea. *Geophysical Journal International*, *203*, 737–754. https://doi.org/10.1093/gji/ggv327

Zhao, C., King, M. A., Watson, C. S., Barletta, V. R., Bordoni, A., Dell, M., & Whitehouse, P. L. (2017). Rapid ice unloading in the Fleming Glacier region, southern Antarctic Peninsula, and its effect on bedrock uplift rates. *Earth and Planetary Science Letters*, *473*, 164–176. https://doi.org/10.1016/j.epsl.2017.06.002